New Journal of Physics
The open-access journal for physics

Mixing via thermocapillary generation of flow patterns inside a microfluidic drop

María Luisa Cordero[1], Hans Olav Rolfsnes[2], Daniel R Burnham[2,3], Paul A Campbell[2], David McGloin[2] and Charles N Baroud[1,4]

[1] LadHyX and Department of Mechanics, Ecole Polytechnique, 91128 Palaiseau cedex, France
[2] Electronic Engineering and Physics Division, University of Dundee, Nethergate, Dundee DD1 4HN, UK
[3] SUPA, School of Physics and Astronomy, University of St Andrews, North Haugh, St Andrews KY16 9SS, UK
E-mail: baroud@ladhyx.polytechnique.fr

New Journal of Physics **11** (2009) 075033 (15pp)
Received 13 February 2009
Published 31 July 2009
Online at http://www.njp.org/
doi:10.1088/1367-2630/11/7/075033

Abstract. The heating produced by a focused laser has been shown to provide a range of manipulation tools on droplets in microfluidic situations, through the generation of thermocapillary flows whose net result is to produce a force on the drop. In particular, droplets of water in oil that are produced in microchannels can be blocked in a special test section. Here, the manipulation of the flow within the droplet is explored through spatial and temporal modulation of the laser pattern used to block the drop. When a stationary pattern of two laser spots is used, the flow preserves the mirror symmetry inside the drop, as happens in the case of two alternating spots if the frequency of the switching is higher than the response rate of the fluid. Lower frequency switching produces a time periodic flow that breaks the mirror symmetry and which leads to efficient mixing inside the droplet. The mixing that is produced by this alternating flow is studied both experimentally and using numerical simulations of particle trajectories from measured velocity fields. This mixing can be optimized for certain parameter ranges, namely by varying the distance between the spots and the forcing frequency.

[4] Author to whom any correspondence should be addressed.

Contents

1. Introduction

The use of droplets was shown, early on, to solve two major problems encountered in microfluidic devices: that of controlling the dispersion of the species, by forcing the chemicals to remain in the drop, and the problem of mixing in the absence of turbulence [1]. Another important advantage of using droplets lies in the ability to readily integrate external manipulation schemes to directly manipulate the liquid, something difficult to achieve with bulk fluid flow. Along these lines, several manipulation tools have been developed whose action is based on using the physical contrasts between the droplet fluid and the surrounding carrier fluid. These techniques have been used to implement fundamental operations on the drops, such as sorting or merging them, either through the contrast of dielectric constant (dielectrophoresis) [2, 3], refractive index [4] or through the manipulation of surface tension by local heating [5, 6].

While most of the above techniques induce recirculation flows within the drop that is being manipulated, previous work has been limited to the study of the net effect on the drop as a whole, rather than on the control of the flow within it. This contrasts with the attention given to mixing in drops as they travel in specially designed channels [1, 7, 8], in suspension outside a microchannel [9, 10], or on a solid substrate [11]. In all of the above cases, chaotic trajectories are obtained inside the drop by combining periodic variations in the recirculation pattern with a mean motion of the drop as a whole. This mean motion was shown to play a major role in breaking the time-reversal symmetry for a particle path, making sure that particles do not return to their initial position at the end of each cycle of the periodic forcing.

Indeed, the main approach to mixing in the absence of turbulence has been to flow fluid particles through chaotic trajectories that are highly sensitive to their initial position [12]. In this way, two particles that are initially close together will separate exponentially, leading to the mixing of particles from different regions of the fluid. This mixing method is not limited to microfluidics; it has been developed in the general case of viscous flows and can be produced through a range of forcing methods and in different geometries [13]. In this approach, the

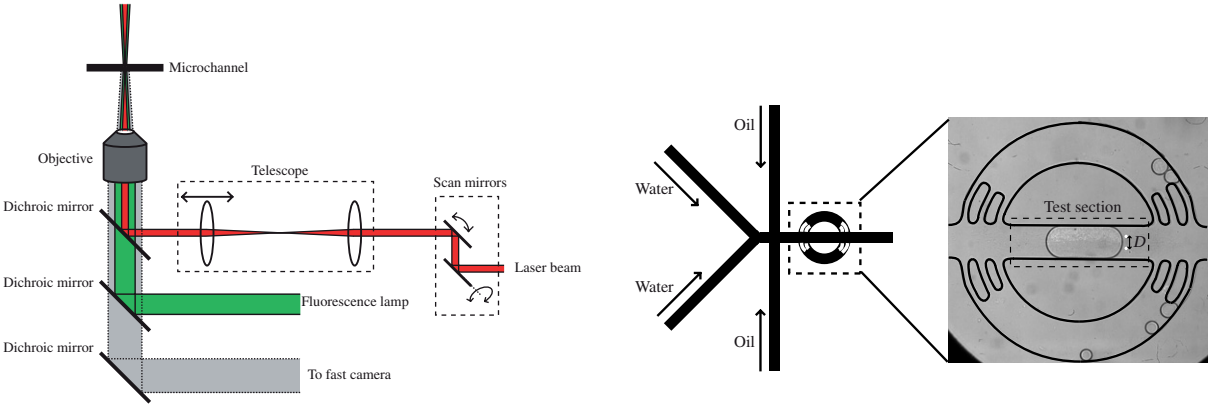

Figure 1. (a) Optical setup with galvanometric mirrors. (b) Microchannel geometry.

aim is to produce a 'stretching and folding' flow, first using the laminar shear flow produced in a viscous fluid (e.g. recirculation rolls inside the translating drops or Poiseuille flow) to separate adjacent particles through a stretching field, then modifying the direction of the flow to reduce the distance over which diffusion takes place ('folding'). In practical situations, the mixing obtained by these mechanisms is enhanced by molecular diffusion and by Taylor–Aris dispersion.

Here we demonstrate that such chaotic flows may be produced in a drop that is held stationary by a focused laser. The mixing properties of the flows created by two different laser configurations are compared: the first configuration uses galvanometric mirrors to produce a time-varying laser pattern that produces a nonstationary flow field. The second configuration uses holographic techniques [14] to produce a stationary laser pattern consisting of two Gaussian spots. In this way, the stationary flow thus obtained is due to the superposition of the velocity fields associated with each of the hot regions. The mean value of the nonstationary flow is similar to the holographically obtained flow. In both cases, the thermocapillary forcing produces the necessary hyperbolic fixed points that lead to the stretching of fluid particles [15, 16]. However, efficient mixing is only obtained in the time-dependent case that breaks the left–right symmetry inside the drop, while the mean recirculation, which does not change sign, breaks the time-reversal symmetry. By contrast, the use of stationary patterns is not sufficient to break the barriers to transport and therefore leads to poor mixing, even though the mean flow given by the switching pattern is the same as the flow given by the stationary pattern.

The two experimental setups used in this study are described in section 2. Section 3 presents the important temporal and spatial scales that must be considered for the problem. The flow fields obtained with each of the laser setups are shown in section 4, followed by the experimental results on mixing that are explained and discussed in section 5.

2. Experimental setups

Two different optical setups are used in this work. The first one, sketched in figure 1(a), is mounted on an inverted microscope (Nikon TE2000) that is equipped with epi-fluorescent illumination (Exfo X-Cite 120). An infrared laser beam (Fitel Furukawa FOL1425) of wavelength 1480 nm is reflected by a pair of galvanometric mirrors (Cambridge Technologies 6210H)

that control the laser position inside the microchannel. The angular position of each mirror can be controlled in real time with custom-made LabVIEW software (National Instruments), allowing us to create nonstationary laser patterns by letting the laser beam alternate between two positions separated by a distance D. The distance between the spots can be controlled with sub-micron resolution and the shifting frequency can be up to 1 kHz. After the galvanometric mirrors, the beam passes through a telescope that consists of an achromatic doublet (Thorlabs, 150 mm focal length) and a convex lens (Thorlabs, 150 mm focal length), both adequate for infrared optics. Then, the laser beam is reflected into the rear aperture of the microscope objective (Nikon Plan Fluor 20X/0.5NA) through a dichroic mirror (OCTAX) and focused inside the microchannel to a 5.3 μm waist [17]. To ensure that the laser is focused at the same plane as visible light, the distance of the telescope is adjusted by moving the achromatic doublet to obtain a slightly diverging beam. Images are recorded with a fast camera (Photron Fastcam 1024 PCI) at frame rates ranging from 250 to 3000 frames per second (fps).

In the second setup, detailed in [14], a 532 nm laser beam is expanded using a telescope to entirely fill the short axis of a spatial light modulator (SLM) (Holoeye LCR-2500), which allows us to holographically shape the laser beam into two stationary Gaussian spots separated by a distance D. Power is controlled using a polarizing beam cube and $\lambda/2$ plate. Two $4f$ imaging systems demagnify the reflected beam into the back aperture of the objective (Nikon 10X/0.25NA), which focuses the beam into the microchannel. Images of the channel are obtained with a firewire camera (Basler A602f) at 240 fps. Kinoforms are generated using a weighted Gerchberg–Saxton algorithm [18], implemented in LabVIEW, to optimize the power uniformity of the spots.

The microfluidic devices are fabricated in polydimethylsiloxane (PDMS) following standard procedures [19] and sealed against a glass slide. The microchannels (figure 1(b)) are 50 μm in height and 200 μm wide. Two independent water inlets merge before the intersection with two oil inlets, where water drops are formed by flow focusing. Liquids are injected using syringe pumps at constant flow rates of 0.04 μl min^{-1} for water and 0.125 μl min^{-1} for oil. Part of the channel is designed to force the drops into a straight test section where they are blocked by the laser, while allowing the oil to bypass the test section through two symmetric secondary channels. At high enough laser power, one drop is blocked until the next drop enters the test section. Therefore, the time duration of the experiments is determined by the frequency of drop formation, which is approximately 1 Hz.

A 50% weight/weight (w/w) paraffin oil–hexadecane mixture is used as the outer phase. A surfactant, Span 80 (Sigma-Aldrich), is added to the oil phase at a concentration of 2% (w/w). When the holographic setup is used, 2% (w/w) ink (dark blue Parker ink) is mixed with the water to increase the absorption of the 532 nm laser beam and therefore heat the water. With the infrared laser this is not necessary due to the high absorption coefficient of the water at 1480 nm.

Micrometer-sized particles are added to the water to be used as tracers. For the first optical setup, green–yellow fluorescent beads (Molecular Probes, 1 μm diameter), at a concentration of 1500 beads per μl, were used to perform particle image velocimetry (PIV) measurements with the use of a commercial software (DaVis, LaVision). These beads yielded images with bright particles in a dark background. For the holographic setup, 4 μm diameter nylon beads were suspended in water, with the aid of surfactant (TX100 (Sigma-Aldrich) at a concentration of 5×10^{-3}% (w/w), i.e. about 0.5 times the critical micelle concentration), to visualize the flows in the absence of fluorescence equipment. These beads appear as dark spots on a light

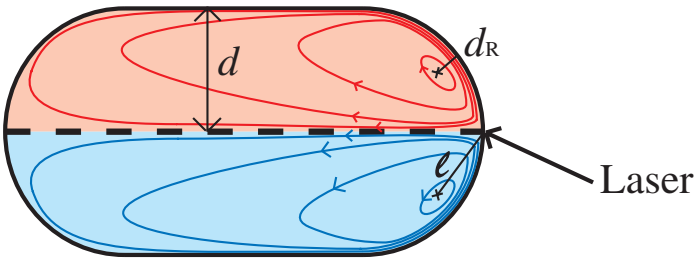

Figure 2. Sketch of the thermocapillary flow pattern inside a drop held by a laser centered in the test channel. The separatrix (dashed line) divides the drop into two regions, corresponding to two counter rotating rolls.

background. In both cases, the images correspond to an average over the vertical dimension because the depth of field of the optics used here are comparable to the channel depth. The nature of the flow is three-dimensional, but the large width to height ratio allows us to assume a parabolic profile, to leading order, in the vertical direction.

In order to quantify mixing efficiency tracers are added to only one of the water inlets and then detected using image analysis. Alternatively, china ink was added to one of the water inlets, in the absence of tracer particles, to visualize the mixing of the droplet contents, using the first optical setup.

3. Temporal and spatial characteristic dimensions

The physics of thermocapillary manipulation and transport involve several spatial and temporal scales and it is useful to recall their values in the case of the present experiments. The efficiency of the mixing will depend on a comparison between the frequency at which the forcing is alternated and the distance between the laser spots with the characteristic scales of the problem.

3.1. Spatial scales

We recall here the main features of the thermocapillary flow field inside a drop that is held by the laser heating (see figure 2). A pair of steady counter rotating recirculation rolls appears inside the drop [20]. The flow at the interface is directed toward the laser position, thus indicating an increase of the surface tension at that location. A separatrix surface separates the rolls and defines two main regions inside the drop on either side of the stagnation points, which remain unmixed, since no streamlines cross the separatrix.

The two inherent spatial scales in the experiments are given by the channel depth and width. The depth can be considered as determining the distance between the edge of the drop and the center of the recirculation rolls (d_R), while the channel width provides the distance d over which a particle must travel to cross from one region of the drop to another.

In the case of optothermal forcing, a thermal length scale around each of the spots must be taken into account. Indeed, it was recently measured that the width of the thermal gradient, $\sigma \simeq 20\,\mu$m, is larger than the laser waist [17]. As a consequence, the distance D between the two laser spots must be larger than 2σ in order to obtain two well-defined temperature peaks in

the case of a stationary pattern. If this is the case, the resulting flow is the superposition of the flows due to each of the temperature fields, owing to the linearity of the Stokes flow. Conversely, if $D < 2\sigma$, the temperature field resembles a single wider hot spot at the front of the drop and the flow field will be similar to the field obtained with a single centered spot.

3.2. Timescales

The first timescale to consider is due to the viscous diffusion that determines the time necessary for the motion of the interface to be felt at a distance ℓ away. Using the distance between the laser position and the center of the recirculation rolls $\ell \simeq 20\,\mu$m [20] as the characteristic length and taking the kinematic viscosity of water $\nu = 10^{-6}\,\mathrm{m^2\,s^{-1}}$, we find $\tau_{\mathrm{visc}} = \ell^2/\nu = 0.4\,$ms. This is the time to propagate the information about the interface motion into the droplet, which will instantaneously lead to recirculating motion by continuity of flow inside the drop, owing to the incompressibility of water.

The second temporal scale is related to the heating of the fluid by the laser. If we assume that the surface tension adjusts immediately to the local value of temperature, the important timescale for creating the thermocapillary motion is due to the time required to produce the thermal gradient [17, 20]. This time is determined by the channel depth and by the thermal properties of the fluids and the channel walls but is independent of the laser power. For the current geometry and fluids, we estimate the heating timescale at $\tau_{\mathrm{th}} \simeq 6\,$ms, as in the case of reference [20].

A third timescale is associated with the transport of fluid particles by the thermocapillary flow. It can be extracted from the characteristic velocity of the interface $v_{\mathrm{int}} \simeq 1\,\mathrm{mm\,s^{-1}}$ and from the half-width of the drop $d = 100\,\mu$m. This advection time $\tau_{\mathrm{adv}} = 100\,$ms represents the time required for a fluid particle to cross between the two regions inside the drop.

The above timescales are well separated with $\tau_{\mathrm{visc}} \ll \tau_{\mathrm{th}} \ll \tau_{\mathrm{adv}}$. Comparing the first two suggests that the limiting time for the fluid to react to the laser is determined by the heating time, i.e. that the thermocapillary flow is established simultaneously with the thermal gradient. Moreover, if the forcing half-period $\tau_{\mathrm{laser}} \ll \tau_{\mathrm{th}}$, the fluid does not have time to cool down between two heating cycles and one expects a stationary convection pattern inside the drop. If on the other hand $\tau_{\mathrm{laser}} \gg \tau_{\mathrm{th}}$, then two independent flow fields are established in an alternating manner simultaneously with the laser switching. In the intermediate range, where $\tau_{\mathrm{laser}} \sim \tau_{\mathrm{th}}$, peaks of temperature periodically occur at the laser positions, forcing the flow in one direction or the other, depending on the strength of the surface tension gradient in each laser position. Finally, τ_{laser} must be larger than τ_{adv} for the mixing to be efficient. If $\tau_{\mathrm{laser}} \ll \tau_{\mathrm{adv}}$, one expects that the flow is too slow to transport particles across the median line and mix them.

4. Flow fields

When a drop is blocked by a single centered laser beam, the flow inside the drop presents a mirror symmetry [20]. The symmetry of this flow is broken when the laser beam is placed at an off-center position, in which case the two recirculation rolls are twisted with respect to the center plane, as shown in figure 3(a) with the aid of fluorescent beads. Toward the rear of the drop the rolls tend to realign parallel to the microchannel, due to the confinement caused by the presence of the channel walls. The velocity field (obtained by PIV) associated with this flow is shown in figure 4(a).

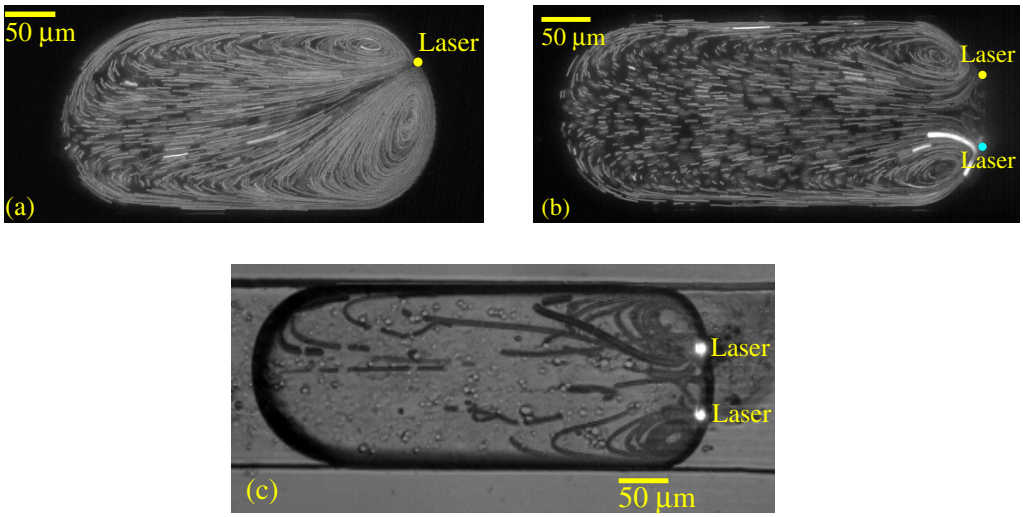

Figure 3. Visualization of the flow fields with tracers in three cases: (a) one off-center laser spot, (b) one rapidly alternating off-center spot (1000 Hz) and (c) two stationary off-center spots.

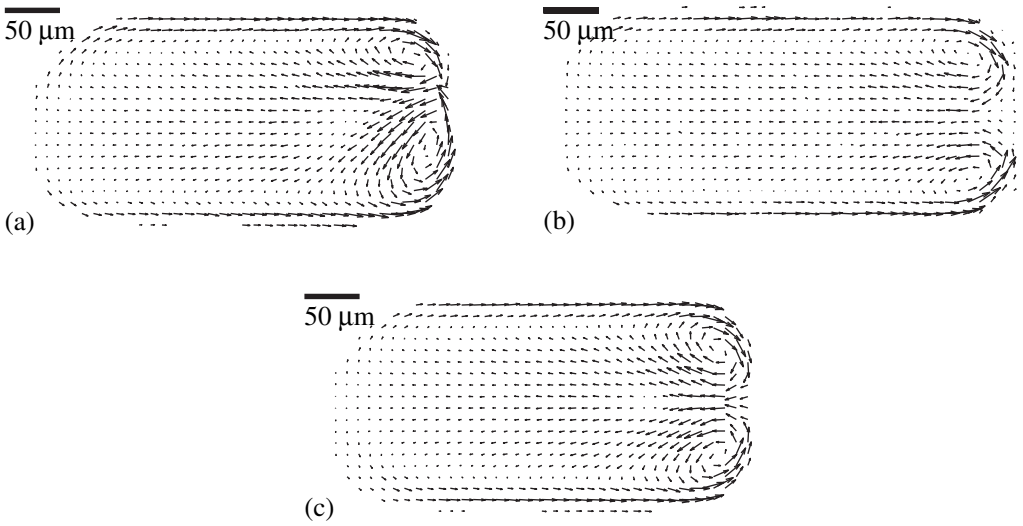

Figure 4. Velocity fields obtained with (a) one off-center laser beam, (b) two rapidly alternating laser spots and (c) the superimposition of the first velocity field and its mirror image with respect to the center plane of the drop.

The flow field obtained with a laser spot that alternates between two symmetric off-center positions depends on the shifting frequency. If the time during which the laser remains in each position $\tau_{\text{laser}} > \tau_{\text{th}}$, a thermal gradient is created alternatively at each of the laser positions, therefore inducing two alternating, asymmetric pairs of recirculation rolls. Neglecting transient effects, whose duration is on the order of the viscous timescale τ_{visc}, the flow switches between the one shown in figure 3(a) and its mirror image with respect to the mid-plane of the drop with half-period τ_{laser}.

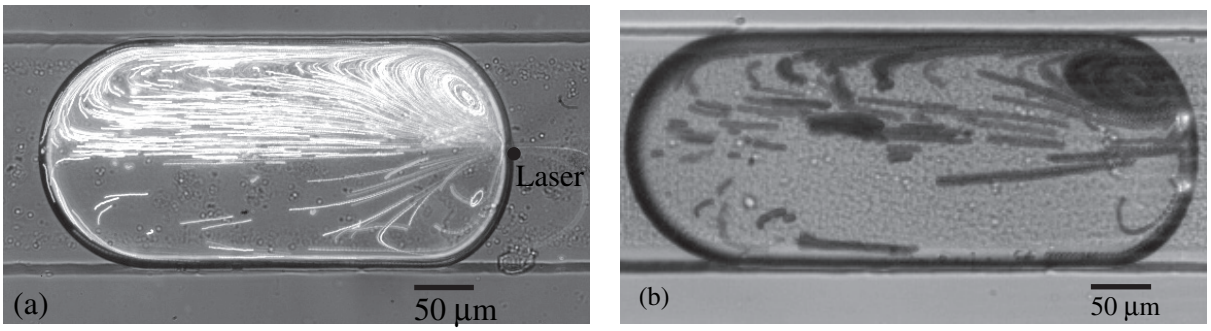

Figure 5. No mixing situation shown by tracers contained in the upper half of a drop blocked by a centered laser beam (a) or by a pair of two symmetric stationary laser spots (b).

If $\tau_{\text{laser}} \ll \tau_{\text{th}}$, a steady thermal gradient is induced by the laser at both positions and a steady thermocapillary flow is created. This flow is shown in figure 3(b) with the aid of fluorescent tracers. Its corresponding velocity field is shown in figure 4(b). The same flow pattern is obtained when a holographically obtained pair of symmetric stationary laser spots is used, as shown in figure 3(c). The flow in these cases recalls the pattern obtained in the presence of one centered laser beam that consists of two large symmetric recirculation rolls that fill the drop. An important difference, however, consists in the presence of two small counter rotating inner rolls between the laser spots near the front interface, which appear because the thermocapillary flow is directed toward each one of the hot spots.

The Stokes nature of the flows allows us to reproduce the velocity field in the presence of two stationary symmetric (or rapidly alternating) laser spots by superimposing the velocity field obtained with one off-center laser spot and its horizontal reflection. The resulting velocity field is shown in figure 4(c), showing good qualitative agreement with the observed pattern (figure 4(b)). The small inner rolls, however, cannot be reproduced because the spatial resolution of the PIV measurements is comparable with the size of these small rolls.

5. Mixing

5.1. Mixing measurements

When tracer particles are added to one of the water inlets two well-separated regions can be distinguished within drops arriving to the test section: one region containing the beads and the other almost without any (some beads are present in the other half of the drop due to fluctuations during the drop formation). As expected, no mixing occurs when the drop is blocked by a single, centered laser beam, and beads remain in the upper half of the drop (figure 5(a)).

In order to measure the mixing efficiency of the flows induced inside the drop by the different laser patterns, the number of beads in each region, $N_{\text{top,bottom}}$, is found as a function of time while the drop is held in the test section. Figures 6(a) and (b) show the cases of two stationary laser spots separated by a distance $D = 16$ and 86 μm, respectively. N_{top} and N_{bottom} remain constant, showing that no mixing occurs. In the first case, the laser spots are close together, so the flow field is similar to the one produced by a single, centered laser beam, as in figure 5(a). For the case of two separated, symmetric laser beams, no mixing occurs either. In fact, the symmetry of the flow field is maintained here, for any value of D, and a symmetry

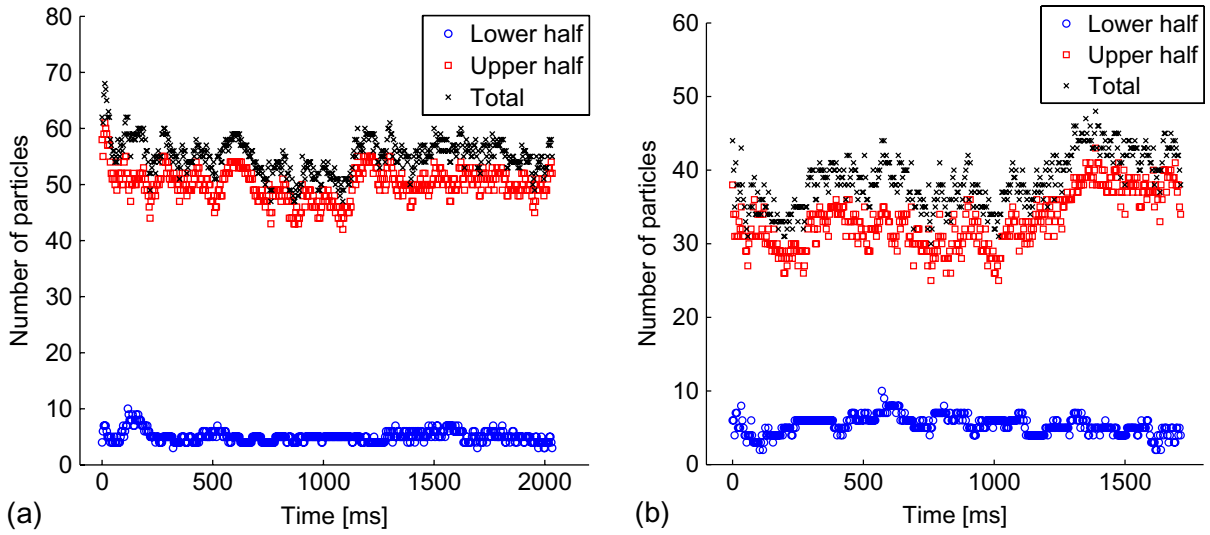

Figure 6. Number of tracers in the upper and lower halves of the drop as a function of time, while the drop is blocked by two stationary laser beams separated by a distance of 16 μm (a) or 86 μm (b).

plane divides the drop in two, keeping the two halves of the drop well separated. This can be observed with the aid of tracers, as shown in figure 5(b).

We repeat the experiment using two alternating laser spots separated by $D = 17$ and 89 μm and with forcing time $\tau_{\text{laser}} = 200$ ms. The number of particles in each half of the drop is shown in figures 7(a) and (b). Again, poor mixing occurs in the first case due to the proximity of the two laser spots, which induce a flow field similar to the one obtained with only one centered laser spot. The use of two beams separated by a larger distance (figure 7(b)), on the contrary, forces particles to cross the mid-plane of the drop, and N_{bottom} decreases progressively as a function of time, while N_{top} increases. After 2.5 s the fraction of particles in each region becomes similar, showing the existence of mixing in this case. Indeed, a necessary condition for mixing is that the number of tracers become equal in both halves of the drop. This is not a sufficient statement of mixing, since it does not ensure the homogeneity within the drop, but once the drop is released from the laser, the recirculation flow associated with the mean motion of the drop can act to mix each of the two halves in the longitudinal direction.

5.2. Mixing efficiency extracted from PIV measurements

From the last section, we observe that the flow field obtained with nonstationary laser patterns can be used to mix the contents of a microdroplet. In fact, divergent trajectories can appear due to the nonstationary flow field, as shown in figure 8 (see also the movie available at stacks.iop.org/NJP/11/075033/mmedia). Here, the velocity field is measured for the case of a laser beam located at a distance $D/2 = 51$ μm with respect to the center of the channel. This is then used to numerically simulate the transport of five imaginary passive tracers. The velocity field is periodically reflected to simulate the switching between the two laser positions, with half-period $\tau_{\text{laser}} = 100$ ms.

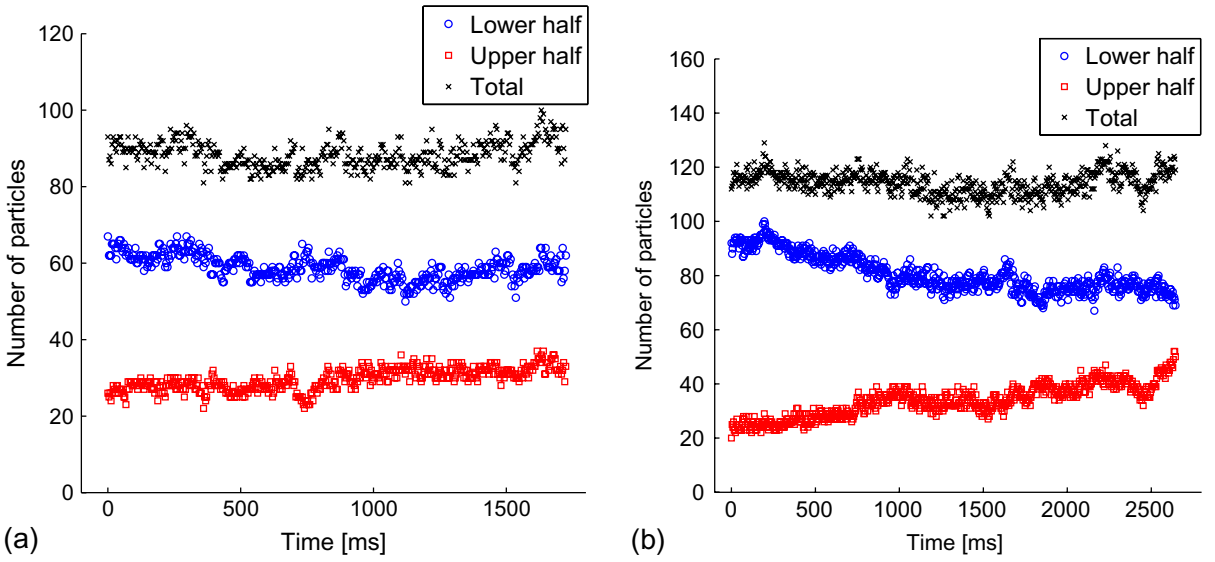

Figure 7. Number of tracers in the upper and lower halves of the drop as a function of time, while the drop is blocked by two alternating laser beams separated by a distance of 17 μm (a) or 89 μm (b). In both cases $\tau_{\text{laser}} = 200$ ms.

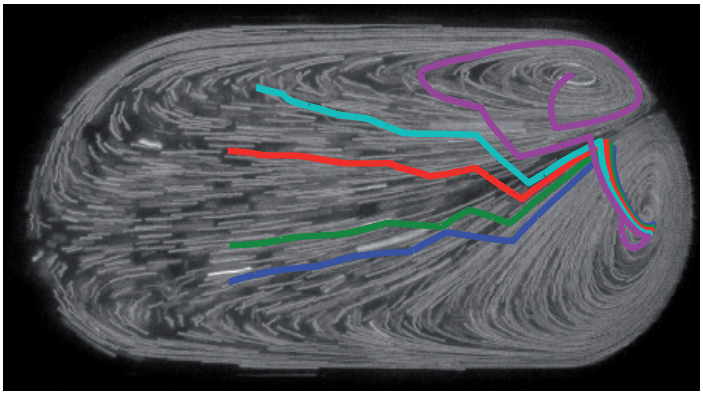

Figure 8. Divergent particle trajectories numerically obtained from PIV measurements.

At $t = 0$ the five particles start aligned within a 5 μm region in the lower part of the drop, near the center of the lower recirculation roll. If the laser position was stationary, one would expect the five particles to remain circulating around the roll center. When the laser alternates between two positions, the switching of the flow field advects the particles far toward the rear of the drop. Moreover, after five periods they finish at distant positions, three of them in the upper half and two in the lower half of the drop. This flow is reminiscent of the 'blinking vortex' flow, which has been shown to produce chaotic mixing [12].

Next, the mixing efficiency is studied as a function of the two parameters of the problem: the distance between the laser spots D and the forcing time τ_{laser}. For this, the trajectory of

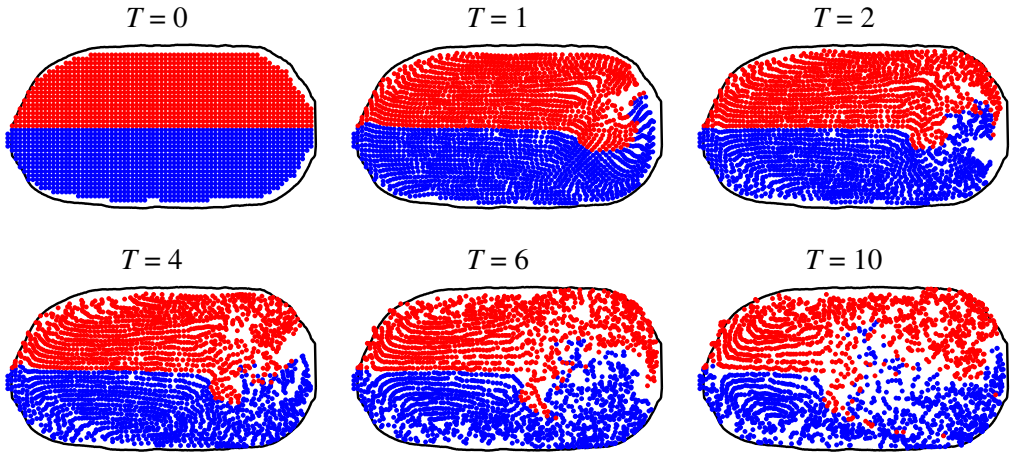

Figure 9. Snapshots of the position of passive tracers as a function of time. Blue (red) spots represent particles placed in the lower (upper) part of the drop at $t = 0$, $D = 102\,\mu$m and $\tau_{\text{laser}} = 100$ ms.

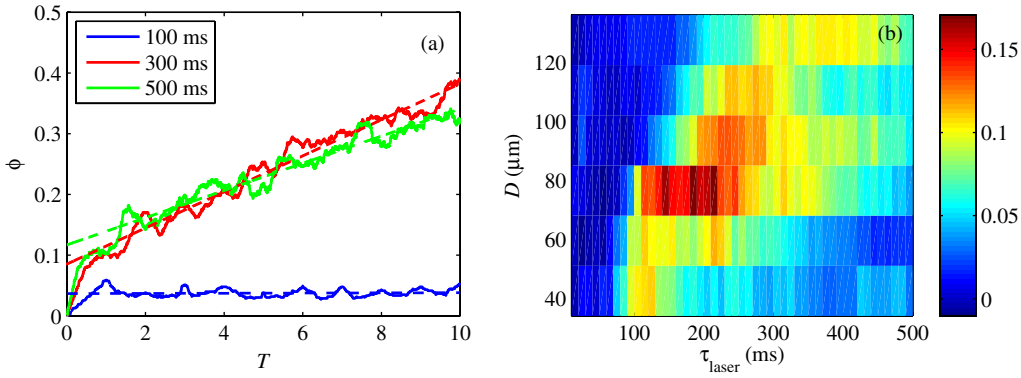

Figure 10. (a) Fraction of particles that cross the mid-plane of the drop as a function of time (solid line), and linear fit (dashed line), for $D = 105\,\mu$m and different values of τ_{laser}. (b) Mixing rate as a function of the distance between the laser spots D and the forcing time τ_{laser}. The scale bar is in units of s^{-1}.

a few thousand passive tracers is calculated as a function of time $T = t/\tau_{\text{laser}}$ between $T = 0$ and 10, for different values of D and τ_{laser}. Figure 9 shows the position of the tracers after different multiples of the half-period T for $D = 102\,\mu$m and $\tau_{\text{laser}} = 100$ ms. Particles starting in the lower half of the drop at $T = 0$ are shown in blue, and particles starting in the upper half are represented in red. As the laser alternates between both positions, 'fingers' of particles cross the mid-plane, penetrating into the opposite half of the drop. These fingers are stretched and advected toward the rear of the drop.

Mixing is quantified by measuring the fraction of particles that cross the mid-plane of the drop, ϕ, as a function of time. $\phi(T)$ is shown in figure 10(a) for $D = 102\,\mu$m and different values of τ_{laser}. The first half-period shows a transient behavior during which many particles cross the mid-plane. This is followed by a linear trend of particle crossings that exhibits periodic peaks of ϕ at the end of each half-cycle.

A mixing rate is extracted from the linear trend as the slope of $\phi(t)$ for $t > \tau_{\text{laser}}$, as shown in figure 10(b) as a function of D and τ_{laser}. For low values of τ_{laser} the mixing is slow, regardless of D, since τ_{laser} is small compared with τ_{adv} and particles do not have time to cross the mid-plane. As τ_{laser} increases, the mixing rate increases, reaching a maximum and then decreasing again for higher values of τ_{laser}. This recalls previous observations of resonant behavior where the forcing time must match an inherent timescale of the system [21]. The global maximum, found for $D = 85\,\mu$m and $\tau_{\text{laser}} = 200$ ms, shows that the mixing is enhanced when the forcing period is in resonance with the advection time τ_{adv} described in section 3.2.

5.3. Mixing of dye

The above results show the mixing of discrete particles within a droplet. Next, we focus on the mixing of dye molecules by adding ink to the lower water inlet. In this way, the drops contain two well-separated regions: a dark half and a clear half, as shown by the first image of figure 11, which shows a drop being blocked by two laser spots separated by a distance $D = 85\,\mu$m that alternate with half-period $\tau_{\text{laser}} = 100$ ms. A similar behavior to what is shown in figure 9 can be observed, with waves of clear and dark liquid being stretched and ejected away from the laser positions (see also the movie available at stacks.iop.org/NJP/11/075033/mmedia).

Figure 11 shows the gray scale difference between the $T = 0$ image and snapshots of the drop after each half-period. Red regions represent clear water waves entering the darker region and blue areas correspond to dark fluid that enters into the clear water. At later T the upper half of the drop becomes darker and the lower half becomes brighter. Similarly to figure 9, the mixed zone is situated next to the laser spots and expands toward the rear of the drop.

6. Discussion

The mixing inside microdrops hinges on the concurrent breaking of several symmetries in the flow field [10]. In the particular case of the confined microchannel geometry, previous work has achieved this by periodically rotating the direction of recirculation rolls with respect to the drop contents, namely by flowing the droplets through a serpentine microchannel [1, 7]. By the same token, the time-reversal symmetry is also broken by the mean motion of the drop. In the case of a drop that is held stationary by thermocapillary action, the time-reversal symmetry is broken by the recirculation rolls that are produced by the laser heating.

Moreover, we show above that mixing does not occur if the forcing is symmetric with respect to the channel width, for example by using holographic patterns that produce a symmetric flow. Even an asymmetric stationary heating pattern would produce poor mixing because of the presence of two separate regions in the drop that do not communicate with each other, as shown by the particle traces. The curved surface, which connects the stagnation points and lies between the two recirculation rolls, forms a barrier to transport that cannot be crossed by fluid particles. Good mixing is therefore only achieved when the separation is modulated, for example by switching between a given forcing pattern and its mirror image to imitate the rotation that has been explored in previous studies.

The mixing efficiency is a complicated function of the forcing parameters, with maximum efficiency occurring for a range of switching frequencies and separations between the forcing points. The presence of this maximum is in agreement with previous results that find resonance conditions for which the mixing is either improved or worsened [22, 23]. Although we do not

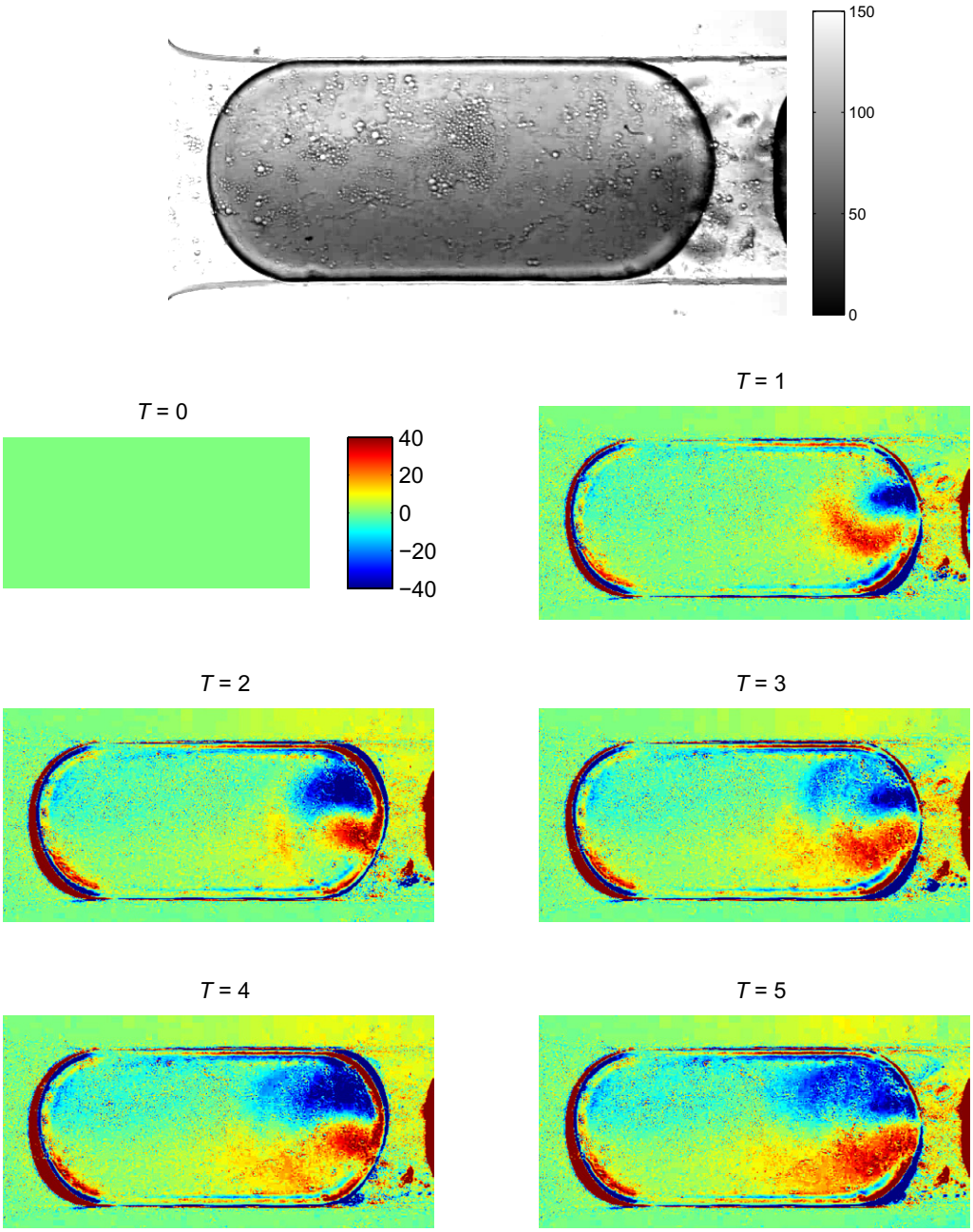

Figure 11. Mixing of ink that is initially present in the lower half of the drop. The first image corresponds to $t = 0$. The consecutive images represent the difference between instantaneous measurements of light intensity and the initial image. Blue means darker, while red means a brighter gray level. After each half-cycle, ink is transported from the lower to the upper half while clear water is transported from the top the half to the lower half. The values of the parameters are $\tau_{\text{laser}} = 100\,\text{ms}$ and $D = 85\,\mu\text{m}$. See corresponding movie available at stacks.iop.org/NJP/11/075033/mmedia. The same color bar applies for $T = 0$–5.

quantify the total quality of the mixing in our drops, the dye experiments show a quasi-total homogenization of the gray levels between the moment that the drop enters and when it exits. Indeed, the dye experiments show that the mixing is further aided by three-dimensional effects and molecular diffusion, which are not accounted for in the numerical study, meaning that the results obtained from figures 9 and 10 are conservative estimates of the true mixing inside the droplets. Three-dimensional effects enhance the mixing in two ways: firstly, the streamlines in the calculations cannot cross since the calculated field is two dimensional. This is not true in a three-dimensional flow field where flow lines do cross at a given projected location but at different heights in the channel. This enhances the mixing by the diffusion of species across flow lines. Secondly, Taylor–Aris dispersion further acts to enhance the mixing, as seen in the dye mixing movie. These three-dimensional effects depend on the diffusion coefficients of the species and should be included in further studies of the mixing.

In the context of droplet microfluidics, the results obtained above are slow when compared with the rates obtained by flowing drops in serpentine channels. For this reason, this approach is not a replacement for passive control of droplets but should be considered as a complementary tool that offers additional modularity. It can be applied at any channel location, which makes it useful for multiple step mixing in order to re-homogenize flowing droplets. Furthermore, the ability to modify the forcing frequency and amplitude can lead to optimized control taking into account the drop size, the fluid viscosities, or the diffusion coefficients. Finally, this approach can provide a way to combine controlled mixing with thermal control, for instance in situations where a chemical reaction is inhibited or enhanced by the heating.

Most importantly, however, these results demonstrate that the laser manipulation tool can serve not only to provide control of the droplet as a whole but also to implement fine control of the flow within it. As such, it forecasts new possibilities in droplet microfluidics and their applications.

Acknowledgments

We thank Romain Lecaque for assistance with the optical setup. This work was partially funded by the British-Council PHC Alliance program. The Polytechnique group was partially supported by grants from Région Ile de France. MLC was funded by the EADS Corporate Foundation and by MIDEPLAN. DM is a Royal Society Research Fellow. PC acknowledges funding through RCUK for a ‘Basic Technology’ award, and also the Northern Research Partnership for a partial funded studentship for HR.

References

[1] Song H, Tice J D and Ismagilov R F 2003 A microfluidic system for controlling reaction networks in time *Angew. Chem. Int. Ed. Engl.* **42** 767–71

[2] Chabert M, Dorfman K D and Viovy J L 2005 Droplet fusion by alternating current (ac) field electro-coalescence in microchannels *Electrophoresis* **26** 3706–15

[3] Ahn K, Kerbage C, Hunt T P, Westervelt R M, Link D R and Weitz D A 2006 Dielectrophoretic manipulation of drops for high-speed microfluidic sorting devices *Appl. Phys. Lett.* **88** 024104

[4] Lorenz R M, Edgar J S, Jeffries G D M, Zhao Y, McGloin D and Chiu D T 2007 Vortex-trap induced fusion of femtoliter-volume aqueous droplets *Anal. Chem.* **79** 224

[5] Baroud C N, Delville J-P, Gallaire F and Wunenburger R 2007 Thermocapillary valve for droplet production and sorting *Phys. Rev.* E **75** 046302
[6] Baroud C N, de Saint Vincent M R and Delville J-P 2007 An optical toolbox for total control of droplet microfluidics *Lab Chip* **7** 1029–33
[7] Stone Z B and Stone H A 2005 Imaging and quantifying mixing in a model droplet micromixer *Phys. Fluids* **17** 063103
[8] Liau A, Karnik R, Majumdar A and Doudna Cate J H 2005 Mixing crowded biological solutions in milliseconds *Anal. Chem.* **77** 7618–25
[9] Ward T and Homsy G M 2001 Electrohydrodynamically driven chaotic mixing in a translating drop *Phys. Fluids* **13** 3521–5
[10] Grigoriev R O, Schatz M F and Sharma V 2006 Chaotic mixing in microdroplets *Lab Chip* **6** 1369–72
[11] Darhuber A A and Troian S M 2005 Principles of microfluidic actuation by modulation of surface stresses *Annu. Rev. Fluid Mech.* **37** 425–55
[12] Aref H 1984 Stirring by chaotic advection *J. Fluid Mech.* **143** 1–21
[13] Ottino J M 1989 *The Kinematics of Mixing: Stretching, Chaos and Transport* (Cambridge: Cambridge University Press)
[14] Cordero M L, Burnham D R, Baroud C N and McGloin D 2008 Thermocapillary manipulation of droplets using holographic beam shaping: microfluidic pin ball *Appl. Phys. Lett.* **93** 034107
[15] Solomon T H and Gollub J P 1988 Chaotic particle transport in time-dependent Rayleigh–Bénard convection *Phys. Rev.* A **38** 6280–6
[16] Voth G A, Haller G and Gollub J P 2002 Experimental measurements of stretching fields in fluid mixing *Phys. Rev. Lett.* **88** 254501
[17] Cordero M L, Verneuil E, Gallaire F and Baroud C N 2009 Time-resolved temperature rise in a thin liquid film due to laser absorption *Phys. Rev.* E **79** 011201
[18] DiLeonardo R, Ianni F and Ruocco G 2007 Computer generation of optimal holograms for optical trap arrays *Opt. Express* **15** 1913
[19] Xia Y and Whitesides G M 1998 Soft lithography *Angew. Chem. Int. Ed. Engl.* **37** 550–75
[20] Verneuil E, Cordero M L, Gallaire F and Baroud C N 2009 Laser-induced force on a microfluidic drop: origin and magnitude *Langmuir* **25** 5127–34
[21] Ward T and Homsy G M 2003 Electrohydrodynamically driven chaotic mixing in a translating drop II. Experiments *Phys. Fluids* **15** 2987
[22] Okkels F and Tabeling P 2004 Spatiotemporal resonances in mixing of open viscous fluids *Phys. Rev. Lett.* **92** 038301
[23] Chabreyrie R, Vainchtein D, Chandre C, Singh P and Aubry N 2008 Tailored mixing inside a translating droplet *Phys. Rev.* E **77** 036314